



## Tree-ring and remote sensing analyses uncover the role played by elevation on European beech sensitivity to late spring frost



Enrico Tonelli<sup>a</sup>, Alessandro Vitali<sup>a,\*</sup>, Francesco Malandra<sup>a</sup>, J. Julio Camarero<sup>b</sup>, Michele Colangelo<sup>b,c</sup>, Angelo Nolè<sup>c</sup>, Francesco Ripullone<sup>c</sup>, Marco Carrer<sup>d</sup>, Carlo Urbinati<sup>a</sup>

<sup>a</sup> Department of Agricultural, Food and Environmental Sciences, Marche Polytechnic University, Ancona, Italy

<sup>b</sup> Instituto Pirenaico de Ecología (IPE, CSIC), Apdo. 202, 50192 Zaragoza, Spain

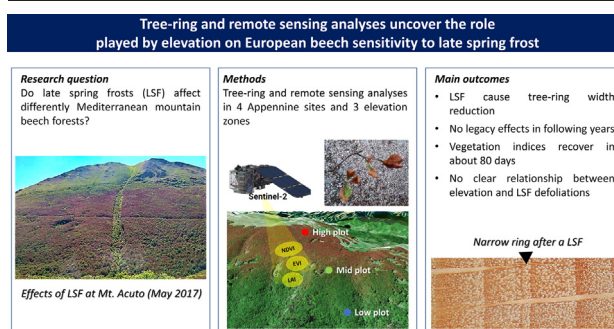
<sup>c</sup> School of Agricultural, Forest, Food and Environmental Sciences (SAFE), University of Basilicata, 85100 Potenza, Italy

<sup>d</sup> Università degli Studi di Padova, Dipartimento Territorio e Sistemi Agro-Forestali (TeSAF), Viale dell'Università 16, 35020 Legnaro, Italy

### HIGHLIGHTS

- Late spring frosts can affect growth of beech in Mediterranean forests.
- Tree-ring and remote sensing analyses applied at four Apennine sites.
- The impact of late spring frost on beech growth depends on site elevation.
- Radial growth resumes after canopy damage without noticeable legacies.
- Remote sensing data reveal canopy recovery after two months from frost event.

### GRAPHICAL ABSTRACT



Tonelli E., Vitali A., Malandra F., Camarero J.J., Colangelo M., Nolè A., Ripullone F., Carrer M. and Urbinati C. (2022)

### ARTICLE INFO

Editor: Manuel Esteban Lucas-Borja

#### Keywords:

Apennines

*Fagus sylvatica*

Dendrochronology

Canopy defoliation

Extreme climate events

Resilience

### ABSTRACT

Extreme climate events such as late spring frosts (LSFs) negatively affect productivity and tree growth in temperate beech forests. However, detailed information on how these forests recover after such events are still missing. We investigated how LSFs affected forest cover and radial growth in European beech (*Fagus sylvatica* L.) populations located at different elevations at four sites in the Italian Apennines, where LSFs have been recorded. We combined tree-ring and remote-sensing data to analyse the sensitivity and recovery capacity of beech populations to LSFs. Using daily temperature records, we reconstructed LSF events and assessed legacy effects on growth. We also evaluated the role played by elevation and stand structure as modulators of LSFs impacts. Finally, using satellite images we computed Normalized Difference Vegetation Index (NDVI), Enhanced Vegetation Index (EVI) and LAI (Leaf Area Index) to evaluate the post-LSF canopy recovery. The growth reduction in LSF-affected trees ranged from 36 % to 84 %. We detected a negative impact of LSF on growth only during the LSF year, with growth recovery occurring within 1–2 years after the event. LSF-affected stands featured low vegetation indices until late June, i.e. on average 75 days after the frost events. We did not find a clear relationship between beech forest elevation and occurrence of LSFs defoliations. Our results indicate a high recovery capacity of common beech and no legacy effects of LSFs.

\* Corresponding author.

E-mail address: [alessandro.vitali@univpm.it](mailto:alessandro.vitali@univpm.it) (A. Vitali).

## 1. Introduction

In temperate forests, a late spring frost (LSF) is an abrupt and severe temperature drop during a period of mild weather (also known as false spring) which negatively impact tree productivity and growth (Augsburger, 2009; Chamberlain et al., 2021). In European hardwood species such as European beech (*Fagus sylvatica* L.) below-zero temperatures during spring can damage the recently unfolded leaves and cause a radial growth reduction (Dittmar et al., 2003, 2006; Gazol et al., 2019; Vitasse et al., 2019; Sangüesa-Barreda et al., 2021). In Mediterranean areas, growth and productivity of beech forests could be also severely constrained by summer drought (Geßler et al., 2007; Piovesan et al., 2008; Gazol et al., 2019; Tognetti et al., 2019; Rita et al., 2020), a factor designing the southernmost xeric edge of beech distribution (Jump et al., 2006; Bolte et al., 2007; Serra-Maluquer et al., 2019; Camarero et al., 2021). In Europe, the recent climate variability significantly increased the frequency of extreme climate events such as LSFs (Augsburger, 2013; Bigler and Bugmann, 2018; Zohner et al., 2020; Lamichhane, 2021) and summer droughts (Spinoni et al., 2018; Gazol and Camarero, 2022; Dukat et al., 2022). In widely distributed species such as beech the combined effects of these extreme climate events pose several questions about forest productivity, tree growth and post-disturbance recovery (Gazol et al., 2019; Vitasse et al., 2019; D'Andrea et al., 2020).

Beech in its juvenile phase is highly vulnerable to LSFs which can cause diffuse seedling mortality, whereas survived individuals could increase their autumn photosynthetic activity (Zohner et al., 2019). In mature beech trees, old carbohydrates can rapidly be mobilized to produce a second cohort of leaves after LSF induced defoliations (D'Andrea et al., 2019). However, new leaves and twigs of affected trees may be smaller and less productive than in undamaged individuals (Rubio-Cuadrado et al., 2021b). Moreover, LSFs occurring in two consecutive years may hamper growth resilience (Rubio-Cuadrado et al., 2021a).

LSF induced defoliations largely depend on the timing of the event occurrence and of the leaf unfolding. Most forest species including beech show earlier spring phenology at lower elevation. Beech bud burst timing is mainly controlled by chilling and forcing temperatures and influenced by the photoperiod length (Heide, 1993; Vitasse and Basler, 2013; Vitasse et al., 2014). Due to the higher chilling requirement, beech at low elevation generally features a delayed budburst compared to the others co-occurring tree species (Vitasse et al., 2009). Also, climate warming affects tree phenology especially at high elevation sites, turning beech forest canopies more prone to LSFs (Čufar et al., 2008; Menzel et al., 2011).

Leaf shedding after LSF is commonly reported in the beech distribution core area, in Central Europe (e.g., Dittmar et al., 2006; Vitasse et al., 2019) and, in recent years, also in Mediterranean mountains at the southernmost beech distribution limit (Gazol et al., 2019). Recent studies, based on remote-sensing and tree-ring data, revealed that LSF defoliation events on southern European beech forests were frequent from 1990 onwards (Olano et al., 2021; Sangüesa-Barreda et al., 2021). Nonetheless, this information could be biased by the availability or quality of satellite images. We need complementary information on how LSF affected beech radial growth in the last decades and across extended ecological gradients, i.e. in sites at different altitudes or with different soil water availability. The Italian Apennine range, due to its geographic layout almost perpendicular to the direction of cold air masses from eastern Europe, provides a valuable setting for such research because appears particularly sensitive to late frost events. Here, beech forest is the most common forest type, spanning from the sub-montane belt up to the upper treeline even at 1900 m a.s.l. (Vitali et al., 2018; Malandra et al., 2019).

In 2016 and 2017 two large-scale LSF events occurred along the Central and Southern Apennines affecting approximately 5000 km<sup>2</sup> of forested area, around one third of the beech forests extension in Italy (Nolè et al., 2018; Bascietto et al., 2018, 2019). LSFs can differently affect beech canopies depending on site elevation and their phenology. A remote-sensing study in Italy indicate that due to later leaf unfolding high-elevation beech forests are less defoliated than mid- and low-elevation stands (Nolè

et al., 2018). However, high elevation stands could be more affected if a late frost occurs at the time of emerging leaves, whereas at lower sites leaves would be more developed and frost resistant.

Lacking a clear relationship between beech forest elevation and occurrence of LSF defoliations, we could reject the hypotheses that: (i) the forests located at higher elevations are more sensitive to LSF disturbance, and (ii) their increased frequency may in the longer term jeopardize the presence of beech from high-altitude sites in Mediterranean mountains. We therefore tested this hypothesis by combining short-term remote sensing information with long-term, retrospective tree-ring analyses at four sites, two located on the wetter central Apennines and two on the drier southern Apennines. The specific multispectral signature of brown-coloured affected foliage after LSF can be detected by satellite imagery and used to assess the geographic extension and the severity of such disturbances at broad spatial scales and in remote sites (Allevato et al., 2019; Decuyper et al., 2020; Olano et al., 2021).

With tree-ring measurements, remote sensing and climatic data, we reconstructed past LSFs and assessed their impacts on beech radial growth and canopy cover and greenness. We aimed (i) to detect the effects of LSF on tree growth along altitudinal gradients, and (ii) to assess the European beech post-LSF recovery and resilience in terms of productivity and canopy greenness with remote sensed imagery.

## 2. Material and methods

### 2.1. Study sites

We studied four locations (Fig. 1) located in central and southern Italy, all within the European beech distribution range (Pott, 2000). In this mountainous region, beech is the most frequent species of the upper treeline ecotones ranging between 1600 and 1900 m a.s.l. (Vitali et al., 2018).

Study sites were selected combining documental evidence of LSF events (e.g., forest reports) with satellite imagery verification (Fig. 1c). Two sites are in the central (Mt. Acuto -ACU and Mt. dei Fiori -MDF), and two in the southern Apennines (Mt. Volturino -VOL and Mt. Pollino -POL), (Table 1, Fig. 1a). At all sites, pure beech forests extend continuously for at least 300–400 m along an elevation gradient from mid-slope to the upper forestline.

Mean annual temperatures range from 8.4 °C (ACU) to 5.0 °C at the coldest location (POL), whereas annual precipitation varies from 754 mm in VOL to 1330 mm in ACU (Table S1). According to the *Ecopedologic map of Italy* all sites are located on calcareous substrates and share the same basic and deep soils (Italian Ministry for the Environment, Land and Sea, <http://www.pcn.minambiente.it/viewer>). Slope steepness ranges between 20 and 40 %, and it increases upwards.

### 2.2. Field data collection

Between 2019 and 2020, in each study site, at high, mid, and low altitude we placed two concentric circular sampling plots (Fig. 1c). Elevation gradients were different at the three sites, according to mountain altitude (Table 1). However, each set of plots (high, intermediate and low elevation) was placed top-down (Fig. 1c) respecting an elevation difference of at least 100 m from one to the others. At each location we sampled beech trees within a larger plot with variable radius between 20 and 30 m to guarantee the presence of at least 20 evenly distributed dominant healthy trees, with  $\geq 30$  cm diameter at breast height (DBH) and without crown damage. The inner plot radius was fixed at 10 m.

In the inner plots we measured the DBH (minimum threshold 2.5 cm) of all standing and living stems. In the larger plots we measured DBH and total height of the dominant individuals with a laser clinometer and rangefinder (TruPulse 360B, Laser Technology, Inc.). In each elevation plot, we extracted wood cores at breast height (1.3 m) orthogonally to the slope from at least 20 dominant trees using a Pressler increment borer. Globally, sample size of increment cores was 303 cores extracted from 244 trees. Basal area ranged from 31 to 77 m<sup>2</sup> ha<sup>-1</sup> and tree height from 13 to

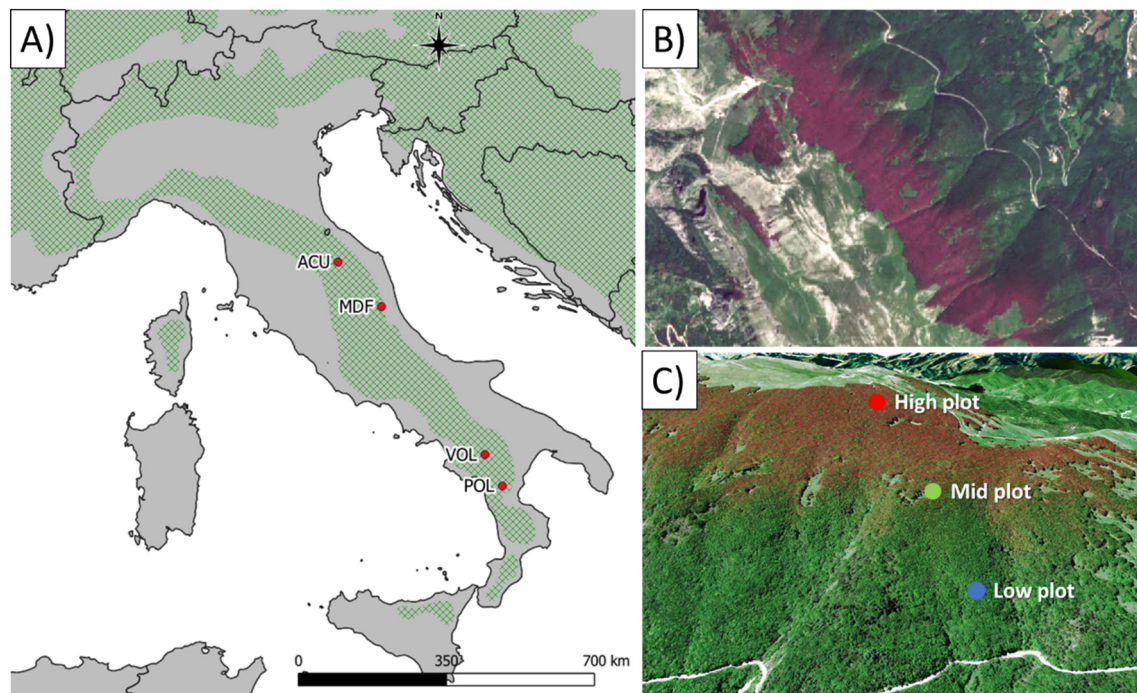


**Fig. 1.** (A) Location of the four study sites in central and southern Apennines (Italy) within the *Fagus sylvatica* distribution range (green area) (Caudullo et al., 2017). (B) A true-colour Sentinel 2A satellite image (May 26th, 2016) showing the beech forest sectors affected by a spring frost at MDF site. (C) Distribution of plot areas along the altitude gradient at MDF, (Google earth Pro V 7.3.4.8248; May 22nd, 2016).

29 m (Table 1). Values variability is partly related to different management systems: overaged coppices (e.g., ACU-high plot) have higher tree density and lower tree size (DBH, height) than high forests (e.g., POL-low plot). Coppices in conversion (e.g., ACU-mid plot) feature intermediate tree density, higher values than high forest and lower than the overaged coppices.

### 2.3. Cores processing and tree-ring width series

We mounted all cores on wooden supports and polished them with progressively finer sandpaper. We visually cross-dated each core and then measured ring widths using a semi-automatic system (LINTAB-TSAP) at 0.01 mm accuracy. We used the COFECHA software to check the visual cross-dating (Holmes, 1983). Then we detrended the tree-ring width series by fitting cubic spline functions to remove the age- and disturbance-related trends and to emphasize the high-frequency growth variability (Cook and

Kairiukstis, 1990). We set the smoothing spline's rigidity at 25 years and its wavelength cut-off value at 50 %. We detrended all measured series dividing observed by fitted values to obtain dimensionless ring-width indices. We averaged individual tree-ring indexed series using a bi-weight robust method to develop a mean chronology and obtained 12 mean plot chronologies (Fig. 2).

We compared the mean chronologies by calculating descriptive statistics both on single raw series, such as the first-order autocorrelation (AC) and the Gini coefficient (Gini), and on indexed series as inter-series correlation (Rbar) and Expressed Population Signals (EPS). The AC describes the influence of the previous growth on the current year growth, and the Gini coefficient accounts for the percentage of variability in the widths from one year to the next (Biondi and Qeadan, 2008), similarly to the mean sensitivity (MS) (Fritts, 1976). Rbar and EPS assess respectively the mean correlation between the series and the similarity degree of a given chronology with a correct reference chronology (Briffa and Jones, 1990; Wigley et al., 1984). We processed the raw series with the “dplR” package (Bunn, 2008) of R software v4.1.2. To assess the similarity among plots' indexed chronologies we calculated their Pearson correlations and performed a Principal Component Analysis (PCA) on the covariance matrix.

### 2.4. Inferring frost events from climate records

To detect the potential LSF years, we used daily climate data from the E-OBS gridded dataset (Cornes et al., 2018), interpolating the temperature records from the grid elevation to the plot location considering a mean lapse rate of  $-6.5\text{ }^{\circ}\text{C km}^{-1}$  as the elevation increases. We used the accumulated degree-days ( $\Sigma T$ ) and chilling requirements ( $C$ ) as proxies of leaf phenology and then spring daily temperature anomalies ( $\Delta T$ ) to quantify the severity of the events.  $\Sigma T$  is the cumulated daily mean temperature above a  $5\text{ }^{\circ}\text{C}$  threshold from January 1st (Day Of the Year - DOY 1) to the date of the minimum temperature recorded between DOY 111 and 131 (approximately from April 20th to May 10th). This method slightly differs from the one in the literature (Vitasse et al., 2019), where accumulated degree-days are accounted to the date of the last late frost day ( $\leq -2\text{ }^{\circ}\text{C}$ ). Yet, to avoid

**Table 1**

Geographic settings of the study sites and their forest structure variables. Forest structure abbreviations: OC, overaged coppice; CC, coppice under conversion; HF, high forest.

Site	Lat (°N)	Long (°E)	Plot	Elevation	Forest structure	Tree density (no stems $\text{ha}^{-1}$ )	Basal area ( $\text{m}^2 \text{ha}^{-1}$ )	DBH (cm)	Height (m)
ACU	43.48	12.68	High	1375	OC	7417	56.47	9.8	13.2
			Mid	1245	CC	1146	44.70	22.3	16.5
			Low	1080	HF	382	77.39	50.8	22.0
MDF	42.79	13.59	High	1584	OC	4170	51.68	12.6	14.9
			Mid	1423	OC	4520	53.98	12.3	15.2
			Low	1159	OC	3342	55.94	14.6	17.3
VOL	40.43	15.79	High	1600	CC	1401	54.69	22.3	21.8
			Mid	1405	CC	1655	49.75	19.6	25.3
			Low	1300	CC	1910	31.72	14.5	20.0
POL	39.93	16.16	High	1890	OC	4010	55.69	13.3	18.8
			Mid	1590	CC	2769	60.30	16.6	20.5
			Low	1450	HF	923	73.35	31.8	29.3

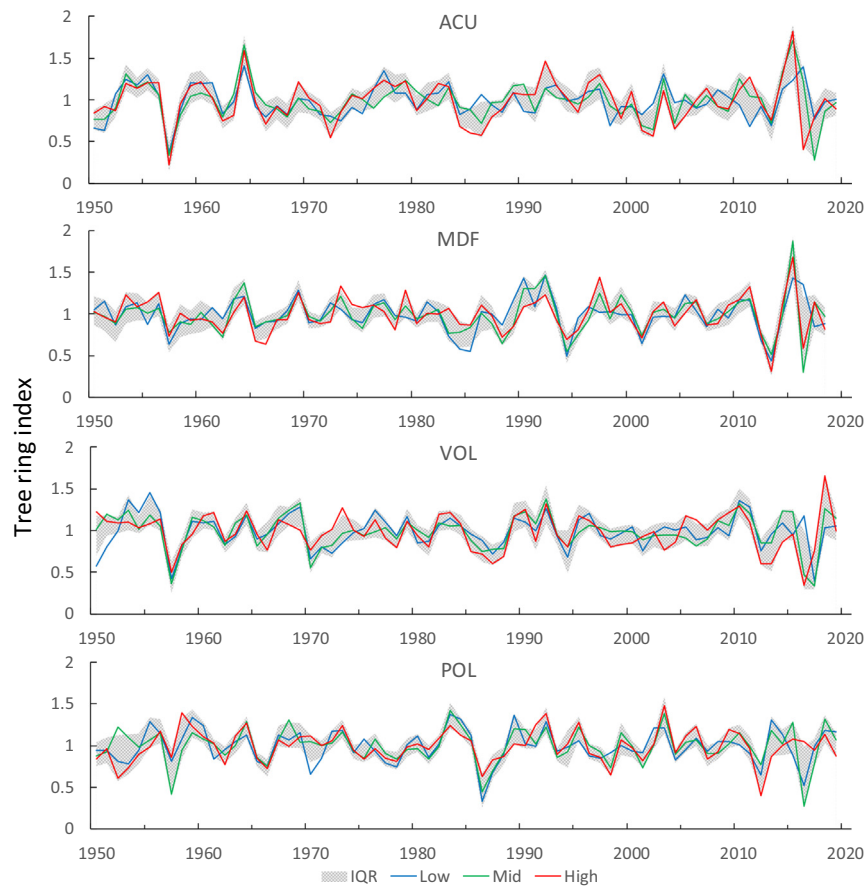


Fig. 2. Mean indexed, ring-width chronologies at high (red), mid (green) and low (blue) elevation plots in the four study sites. The grey shadow is the interquartile range (IQR) of each site series. Chronologies are truncated in 1950 for matching the common period used for the detection of LSF years (1950–2019).

influences related to temperature interpolation in gridded datasets, which are prone to large errors, especially in daily records and across topographically complex areas, we decided to consider the day with minimum temperatures rather than the temperature threshold of  $-2^{\circ}\text{C}$ . Chilling requirement was calculated as days with mean air temperature  $<10^{\circ}\text{C}$  between November 1st to the date of the minimum temperature recorded between DOY 111 and 131 (the same period used for the calculation of the  $\Sigma T$ ).

For the LSF detection, we computed spring temperature anomalies ( $\Delta T$ ) or the difference between the mean minimum temperature from March 1st to April 30th and the minimum temperature from April 20th to May 10th for each year. High values of  $\Sigma T$  and  $\Delta T$  lead to a higher probability for beech to suffer LSF events (Gazol et al., 2019; Vitasse et al., 2019). We defined years with the highest risk of severe LSF when both  $\Sigma T$  and  $\Delta T$  exceeded the 3rd quartile computed for the reference period 1951–1990. While  $\Sigma T$  temperatures cannot be effective if the chilling requirement is not reached, the years selected must guarantee at least 120 days of C index (Dantec et al., 2014).

We then compared these three meteorological indices ( $\Sigma T$ ,  $\Delta T$  and  $C$ ) and validated them with available daily data collected by local meteorological stations (Table S2). Again, temperature records were interpolated from station elevation to the plot location considering a mean lapse rate of  $-6.5^{\circ}\text{C km}^{-1}$ . Local stations provide the daily absolute minimum temperatures that we used to validate the calculated  $\Delta T$  values considering only the frost events (temperature  $< 0^{\circ}\text{C}$ ).

## 2.5. Quantifying frost impacts on tree growth

In dendrochronology an event year is a dated tree-ring considerably wider or narrower with respect to prior or subsequent rings, whereas a

pointer year refers to several trees that display synchronously an event year within the series (Schweingruber et al., 1990). If LSFs are sufficiently severe, they can affect the cambial activity of trees and induce the formation of narrow rings detectable as negative event years and possibly as pointer years. We computed pointer years of all indexed individual tree-ring width series with the “Normalization in a moving Window” method (Cropper, 1979) using the R package PointRes (van der Maaten-Theunissen et al., 2015). This method delivers Cropper values ( $z_i$ ) series by normalizing tree-ring width series in moving windows. We considered event years  $|z_i|$  values of 0.75 in a 5-year moving window. We retained a pointer year when the event year occurred in 75 % of the plot series. Then, we selected the negative pointer years (nPYs) matching with a LSF year.

We estimated the recovery time after the selected years on indexed tree-ring width series using the Superposed Epoch Analysis (SEA), with a time lag of 4 years and bootstrapped resampling (Lough and Fritts, 1987), using the “sea” function of the “dplR” package (Bunn, 2008). Then, we averaged and plotted the departures from the mean SEA value of each core for the 4 years prior to, and immediately after each LSF nPY, to determine the occurrence of significant growth deviations. This analysis allows detecting post-frost carryover or legacy effects on radial growth. For the SEA over recent LSFs occurring in 2016 and 2017 we considered only one or two years after each event, since tree-ring series end in 2018 (MDF site) or 2019 (ACU, VOL and POL sites).

As an additional analysis to assess the impact of LSF in nPYs, we calculated resistance ( $R_t$ ), recovery ( $R_c$ ) and Resilience ( $R_s$ ) indices following Lloret et al. (2011):

$$\text{Resistance (Rt)} = \text{Ring width index}_t / \text{Ring width index}_{t-2} \quad (1)$$

$$\text{Recovery (Rc)} = \text{Ring width index}_{t+2} / \text{Ring width index}_t \quad (2)$$

$$\text{Resilience (Rs)} = \text{Ring width index}_{t+2} / \text{Ring width index}_{t-2} \quad (3)$$

We computed these indices using standard tree-ring width series and a 2-year lag to avoid recovery underestimation due to consecutive LSFs, and to study the most recent LSFs.

### 2.6. Tree variability to frost sensitivity

The effect of various drivers of individual tree growth on frost sensitivity was analysed at tree level. We assumed that beech sensitivity to spring frost could be explained by individual tree characteristics, such as cambial age and topographic elevation that could play an important role. The total number of LSF rings obtained by climate data analysis was considered as an indicator of frost sensitivity. We fitted Generalized Linear Mixed-effects Models (GLMMs) for predicting at each site the number of LSF rings formed by each tree as a function of the following variables: cambial age, mean tree-ring width, basal area increment (BAI), mean sensitivity and Gini index computed for the period 1950–2019, and the growth trend (based on the slope of BAI) in the period 1990–2019. From the analysis we removed BAI from the predictors because it showed a high ( $\geq 4$ ) Variance Inflation Factor, to avoid multicollinearity among the independent variables. We rescaled all the predictors to account for differences on measurement scale and we used a Poisson distribution family for the response count variable (LSF rings). For each model, we also used the plot elevation as random factor to search for different responses among plots.

We fitted two GLMMs for modelling the presence/absence of LSF rings in each series in 1957 and 2016, the years with more trees affected by frost, as a function of cambial age, mean tree-ring width, mean sensitivity, and Gini index. We used plots nested in sites to focus on the explained variance. We rescaled all the predictors to account for differences on measurement scale and we used a binomial distribution family for the response variable (presence/absence of LSF rings). We performed all statistical analyses within the R environment, using the “glm” function of “stats” package (version 4.0.3) and the “glmer” function of “lme4” package (Bates et al., 2015). BAI was calculated using the “bai.out” function of the “dplr” package (Bunn, 2008).

### 2.7. Frost events detected through remote sensed imagery

We used multispectral satellite Copernicus Sentinel-2 imagery to estimate the incidence of late frost and the recovery time of beech at the different plots. We used images from the twin satellites Sentinel-2A and Sentinel-2B. These platforms carry a Multi-Spectral Instrument (MSI) that samples thirteen spectral bands (Drusch et al., 2012). The EO Browser service (<https://www.sentinel-hub.com/explore/eobrowser/>) allowed satellite images selection with cloud-free areas over the study sites for the time interval ranging from March 2016 to December 2018. We selected images only for ACU and VOL sites due to (i) the least cloud contamination over their plots, and (ii) the occurrence of two consecutive LSF events in 2016 and 2017. We collected 62 images of the same time interval and downloaded the corresponding products from the Copernicus Scientific Data Hub (<https://scihub.copernicus.eu/>) as a Level-1C (Top-of-atmosphere reflectance – orthoimage products) and Level-2A (Bottom-of-atmosphere reflectance – atmospherically corrected), when available (Table S3).

We processed twenty-six Sentinel-2 Level-1C images performing the atmospheric corrections using the Sen2Cor V2.8 processor and SNAP 8.0 software provided by the European Space Agency. We used the classification mask, built from the scene classification layer produced by Level 2A-processing, or provided in the Level 2 product acquired, to remove pixels classified specifically as cloud shadows, water, intermediate and high-probability of cloud cover, thin cirrus, and snow. All images were calibrated to convert Digital Number into units of surface reflectance applying their respective scale factor. Then we calculated three vegetation indices: (i) Normalized Difference Vegetation Index (NDVI), (ii) Enhanced

Vegetation Index (EVI), and (iii) Leaf Area Index (LAI). NDVI is the most widely used vegetation index and it is not only related to canopy structure and LAI, but also to canopy cover and greenness (Xue and Su, 2017). NDVI ranges between  $-1$  and  $1$  (Rouse et al., 1973) and is computed as follows:

$$\text{NDVI} = (\text{NIR} - \text{Red}) / (\text{NIR} + \text{Red}) \quad (4)$$

where NIR and Red are reflection values in the near-infrared and red ranges of the electromagnetic spectrum. Positive NDVI values between 0.3 and 0.8 usually refer to vegetation canopy with a high cover and greenness values. Since NDVI is sensitive to soil brightness and atmosphere conditions, EVI can simultaneously correct these noises (Liu and Huete, 1995; Huete et al., 2002). EVI is expressed as:

$$\text{EVI} = G * (\text{NIR} - \text{Red}) / (\text{NIR} + \text{C1} * \text{Red} - \text{C2} * \text{Blue} + \text{L}) \quad (5)$$

where G is the gain factor, L the soil adjustment parameters, C1 and C2 are the coefficients used to correct the aerosol influences in the red band, and Blue are reflection values from the blue band. For the Sentinel 2 products, according to Henrich et al. (2009), we adopted the following coefficients:  $L = 1$ ,  $C1 = 6$ ,  $C2 = 7.5$ , and  $G = 2.5$ .

For each selected image, we computed NDVI and EVI in a 40-m radius buffer zone from each plot centroids. A minimum of 30 pixels falling within the 40-m buffer were used to extract NDVI and EVI mean values for each low, mid, and high elevation plots at both ACU and VOL sites.

Finally, effective Leaf Area Index ( $\text{LAI}_{\text{eff}}$ ) was estimated from satellite observations using the biophysical processor in SNAP 8.0. This function is proposed to use neural networks for the estimation of biophysical variables (Weiss and Baret, 2016). We calculated the  $\text{LAI}_{\text{eff}}$  at ACU and VOL sites on the date of maximum LSF severity and on the date of the following full recovery time.

## 3. Results

### 3.1. Tree growth

Mean tree age varied from 61 years to 132 years, with the oldest tree (216 years) sampled at the VOL-high plot (Table 2). The mean tree-ring width ranged from 1.39 to 2.10 mm. At ACU, trees at low elevation showed the highest mean growth rate, but the rate decreased with increasing elevation (Table 2, Fig. S1). The MDF, VOL and POL plots have similar growth rates within each site with no evident effects due to elevation, although the POL-low showed lower growth rates after 1990 (Fig. S1). At MDF, we found wider rings in the lowest plot, whereas in VOL and POL at the mid-elevation plots.

First order autocorrelation values (AC1) in tree-ring width series are similar and ranging between 0.51 and 0.74 (Table 2). High Gini coefficients

**Table 2**  
Dendrochronological statistics of sampled trees. First-order autocorrelation (AC1) and Gini (Gini) coefficients refer to the raw series, whereas inter-series correlation (Rbar) and Expressed Population Signal (EPS) refer to indexed ring-width series. Values are means  $\pm$  SD.

Site plot	No. trees	Series length (yrs.)	Ring width (mm)	AC1	Gini	Rbar	EPS
ACU-High	23	75 $\pm$ 11	1.03 $\pm$ 0.48	0.51	0.25	0.50	0.94
ACU-Mid	18	85 $\pm$ 14	1.51 $\pm$ 0.66	0.57	0.25	0.34	0.88
ACU-Low	17	104 $\pm$ 14	2.18 $\pm$ 0.93	0.61	0.24	0.37	0.90
MDF-High	18	75 $\pm$ 19	1.56 $\pm$ 0.66	0.50	0.23	0.43	0.90
MDF-Mid	20	71 $\pm$ 8	1.42 $\pm$ 0.65	0.57	0.25	0.43	0.92
MDF-Low	20	61 $\pm$ 6	1.80 $\pm$ 0.82	0.63	0.25	0.44	0.93
VOL-High	26	120 $\pm$ 46	1.66 $\pm$ 0.80	0.62	0.28	0.35	0.88
VOL-Mid	27	75 $\pm$ 28	2.10 $\pm$ 1.08	0.62	0.28	0.34	0.86
VOL-Low	26	111 $\pm$ 58	1.54 $\pm$ 0.86	0.69	0.32	0.37	0.87
POL-High	25	108 $\pm$ 48	1.59 $\pm$ 0.81	0.67	0.29	0.35	0.88
POL-Mid	27	84 $\pm$ 33	1.87 $\pm$ 0.81	0.55	0.25	0.40	0.90
POL-Low	22	133 $\pm$ 30	1.39 $\pm$ 0.77	0.74	0.31	0.32	0.88

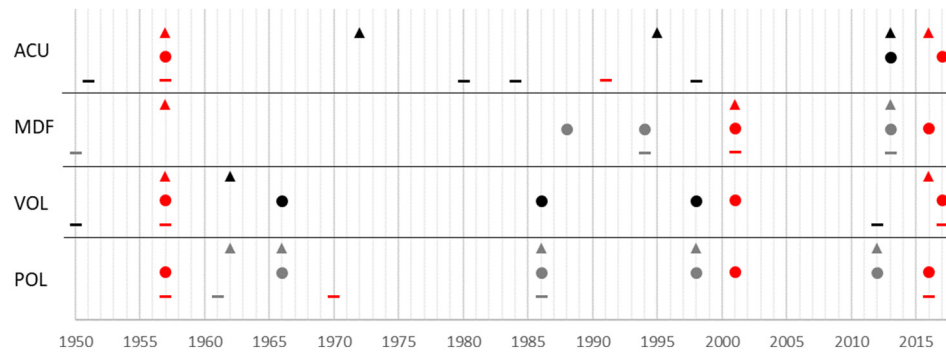


**Fig. 3.** Negative pointer years (nPYs) detected at high (▲), mid (●) and low (–) elevation plots of the four study sites in the period 1950–2019. In red the nPYs occurred in LSF years when  $\Delta T$  and  $\Sigma T$  exceeded the third quartile threshold.

indicate sensitive series with high year-to-year growth variability. The EPS and Rbar values are high at all sites suggesting a large inter-annual growth variation and synchrony, i.e., a common growth signal shared among trees. Tree-ring chronologies developed at each site at different elevations are positively correlated with high and significant ( $p < 0.01$ ) correlation values (Table S4). Similarly, the PCA discriminates two groups of plots mean chronologies corresponding to the central and southern Apennines (Fig. S2). Their yearly interquartile range (IQR) reached the highest values in years of LSF occurrence, such as 2016 and 2017 (Fig. 2). In these two years, very cold spring temperatures reduced growth rates of several trees. We also observed other abrupt growth reductions in most trees related to LSFs in 1957 and 2001 (Fig. 2).

### 3.2. Detection of LSF years using temperature data

The analysis of climate records revealed eleven potential LSF years (1955, 1957, 1962, 1967, 1970, 1977, 1989, 1991, 2001, 2016 and 2017). In these years, accumulated degree days ( $\Sigma T$ ) and spring temperature anomalies ( $\Delta T$ ) exceeded the threshold values of the third quartile computed for the 1951–1990 reference period (Fig. S3, Table S5) while the chilling requirements ( $C$ ) exceeded 120 days. In four years (1957, 1991, 2016 and 2017) there is documented evidence of frost events, and local climate records confirm the abrupt drop of temperatures (Table S6). In 1957, 1991 and 2017, high temperature anomalies were recorded at all sites, whereas in 2016 E-OBS data underestimated the frost risk for the southern VOL and POL sites. Above average  $\Sigma T$  and  $\Delta T$  values following the LSF events in years 1957, 2016 and 2017 are recorded in most sites and plots, whereas in 1991 high  $\Sigma T$  and  $\Delta T$  occurred only at ACU site.

### 3.3. Impact of LSF on radial growth

Within the common period 1950–2019 we detected 56 nPYs distributed in 21 different calendar years (Fig. 3). In particular, 24 nPYs were associated to LSF events detected in previous analyses. LSF rings occurred in 1957, 1970, 1991, 2001, 2016 and 2017. All trees from ACU and VOL sites showed the 1957 nPY, as well as the MDF-high, POL-low and POL-mid plots. The LSF events in 1970 and 1991 lead to nPYs only in POL-low and ACU-low plots, respectively. All MDF plots shared a LSF ring in 2001, as well as VOL-mid and POL-mid plots. According to local climate station data, the mean values of  $\Sigma T$ ,  $C$  and absolute minimum temperatures in years of LSF ring occurrence were 302 °C, 168 days and  $-3.9$  °C respectively (Fig. S4).

The SEA of ring-width indexed series revealed a significant ( $p < 0.05$ ) growth reduction in 71 % of the series during the LSF years (Fig. 4). One year after each LSF event growth was recovering since reduction occurred in only 4.9 % of the trees. In affected trees average growth was 54 and 84 % lower than the two preceding years (Table S7). At all plots, growth series showed high levels of recovery. Two years after ( $t_{+2}$ ) the LSFs, tree rings were 2.49–4.81 times wider than in the year of the event. The resilience index was around 1 or even higher in most cases, meaning that ring-width indices were equal or higher in  $t_{+2}$  compared to  $t_{-2}$ . Only at ACU, the resilience index showed low values, in mid-elevation plots after the 2017 LSF (Table S7).

### 3.4. Variability factors in growth sensitivity to LSFs

Several trees featured some narrow rings related to spring frost (LSF rings). The frequency of LSF rings ranged from zero to five in the period

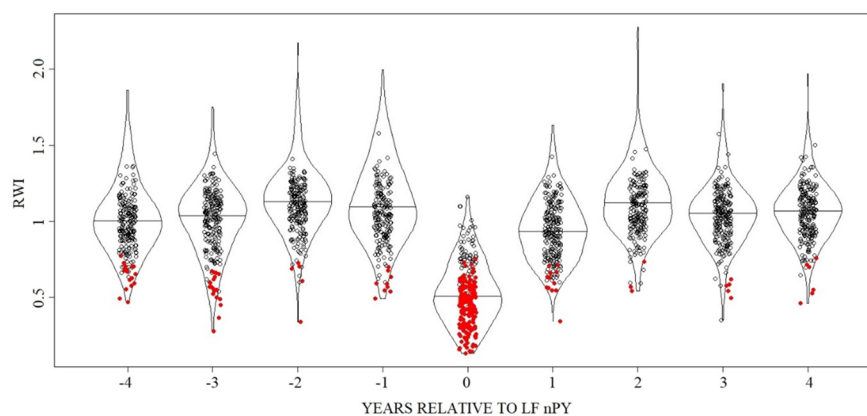


**Fig. 4.** SEA beech growth response to spring late frosts (LSFs) in 1950–2019. The y axis shows the number of years before and after LSF negative pointer years (nPY). Horizontal lines inside the “violins” indicate median ring-width indices (RWI), whereas red dots correspond to significant ( $p < 0.05$ ) RWI reductions.

1960–2019, with most trees (41.8 %) showing two LSF rings in their tree-ring series (Fig. S5). The estimated number of LSF rings tends to be higher at mid- than at low- and high-elevation plots (Fig. S6), but between-plot differences tend to be significant only at MDF site ( $p = 0.11$ ). We did not find any significant contribution of tree parameters such as age, mean TRW, MS, Gini, and BAI trend as predictors of the LSF rings number using the GLMMs modelling approach (Table S8). We found only two significant predictors using binomial models with random effects (GLMMs) to predict presence/absence of frost in 1957 (Age) and 2016 (Gini). For the 1957 events, the sites explained 66 % of variance, while plot elevation only 6 % (Table S6).

### 3.5. Late frost detection from remote sensing data

We computed vegetation indices (NDVI, EVI and LAI) at each elevation plot in ACU and VOL sites to assess the canopy reflectance trend throughout the growing seasons in 2016 and 2017 (years with LSF) as compared with 2018, a LSF free year (Figs. 5 and 6). At ACU, the 2016 frost occurred on April 26th (DOY 116) and affected only the high-elevation plot. NDVI and EVI values were respectively 25 % and 43 % lower than unaffected plots at DOY 147. EVI and NDVI values recovered over two months (DOY 180). At the same site, in 2017 the LSF occurred on April 22nd (DOY 112) and affected only the mid-elevation plot, with NDVI and EVI values respectively 65 % and 51 % lower than undisturbed plots at DOY 151. At ACU in 2017 beech canopies fully recovered the LSF event after 79 days (DOY 191), when spectral vegetation indices assume the same levels as the unaffected plots. The LSF occurred at VOL in 2016 (DOY 116) affected the high-elevation plot, with NDVI and EVI values respectively 34 % and 54 % lower

than undamaged plots at DOY 144. On the contrary, the 2017 LSF (DOY 111) affected only the low- and mid-elevation VOL plots, with NDVI and EVI values respectively 17 % and 23 % lower than at unaffected high-elevation plot at DOY 134. At VOL LSF in affected plots EVI and NDVI reached normal values after 88 days in 2016 and after 67 days in 2017.

Late spring frost effect on  $LAI_{eff}$  is evident at both ACU and VOL in 2016 and 2017. We found differences comparing mean values of affected and unaffected plots and between post-frost (DOY 140–160) and recovery periods (DOY 190–210). In affected plots, the  $LAI_{eff}$  values are nearly half of those recorded in unaffected plots ( $1.2$  to  $2.3$   $m^2 m^{-2}$  vs.  $2.8$ – $5.0$   $m^2 m^{-2}$ ) (Fig. 6). As expected, in the latter plots  $LAI_{eff}$  values of post-frost and recovery periods were very similar, whereas in affected plots  $LAI_{eff}$  increased until mid-July and reached  $3.2$ – $4.0$   $m^2 m^{-2}$  values. However, in disturbed plots estimated  $LAI_{eff}$  in the recovery period are in most cases slightly lower than in undisturbed plots.

## 4. Discussion

The Apennines range, where beech shares over 10 % of the total forested area, is a transition zone where cold and wet air masses coming from Northern and Eastern Europe are merging with warm and dry masses from Northern Africa. These conditions can induce important regional or local phenological variability of beech and increase its sensitivity to LSF events. Here we focused on detection and assessment of LSF effects on beech stands in Central and Southern Apennines. We used diverse but complementary approaches to quantify, date, and spatially define the occurrence and the effects of major LSFs on beech forest productivity and

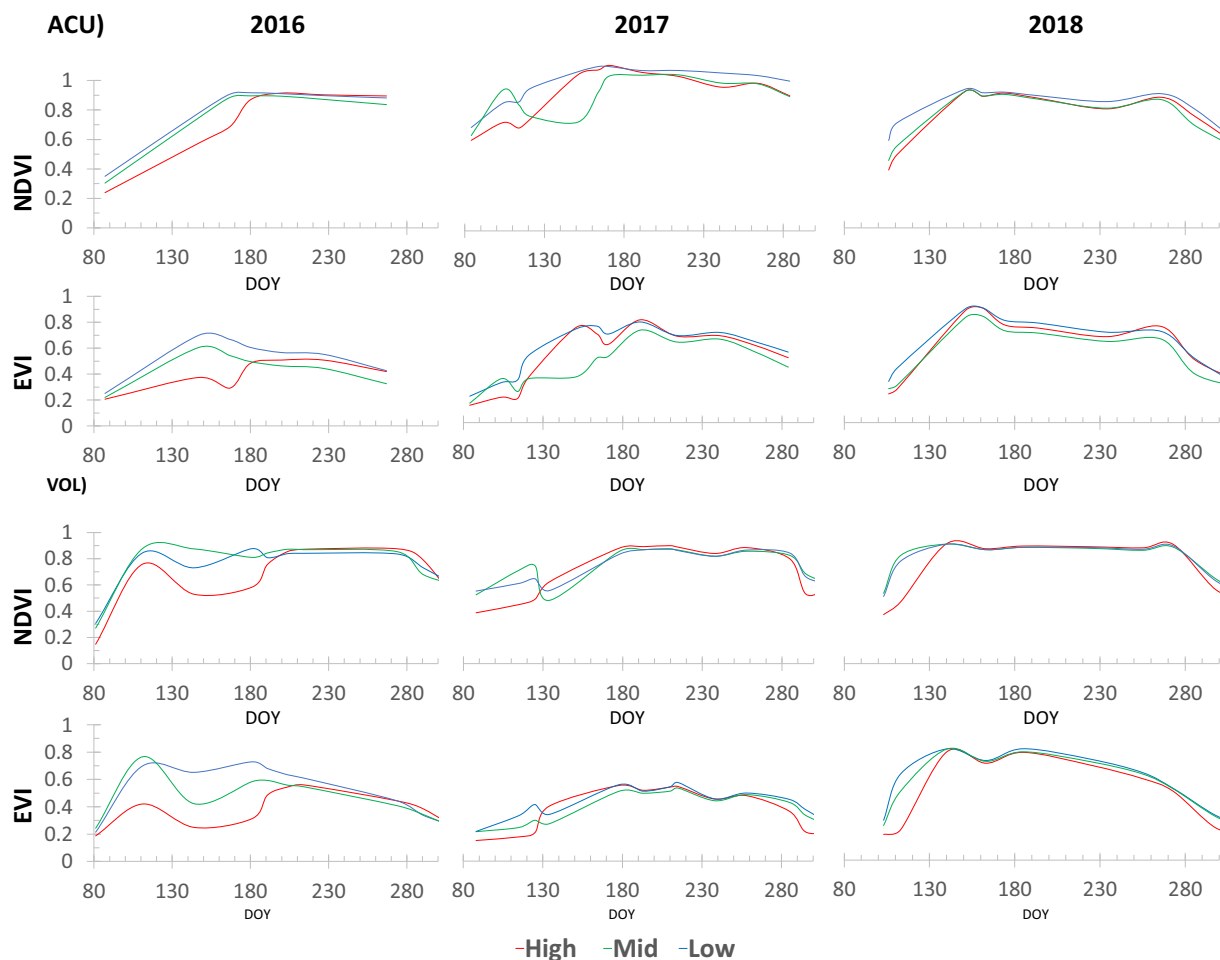


Fig. 5. The averaged NDVI and EVI trend curves throughout the growing seasons in 2016 and 2017 (LSF years) and 2018 (no-LSF year) at the three elevation plots at ACU and VOL sites. DOY (day of the year) is reported in x axes.

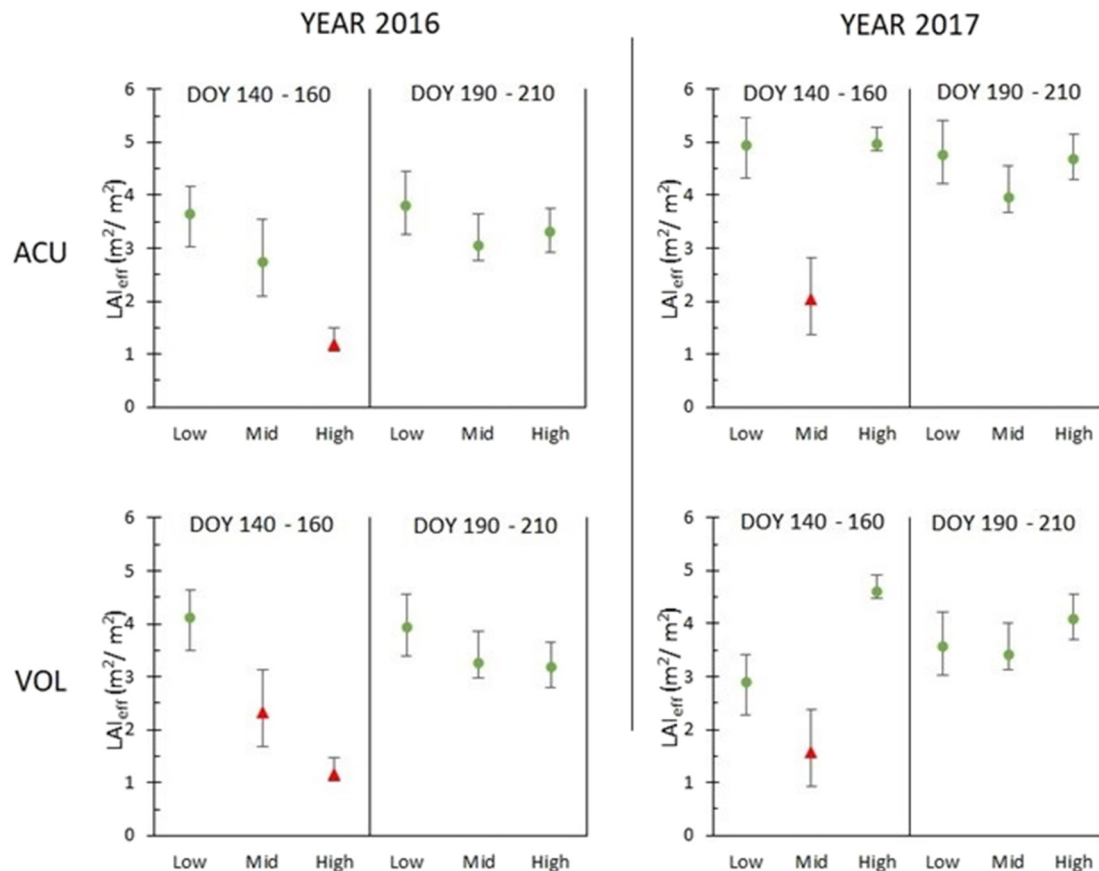


Fig. 6. LAI<sub>eff</sub> values at ACU and VOL sites in two LSF years (2016 and 2017). The whiskers represent the minimum and maximum values within each plot. Mean LAI<sub>eff</sub> values were compared between plots using a two-sided Wilcoxon test. Significantly ( $p < 0.01$ ) low LAI<sub>eff</sub> values in affected plots are marked with a red triangle.

growth. The results confirmed our hypothesis of the absence of a clear relationship between beech forest elevation and the incidence of LSF-induced defoliation. More severe growth reduction was found at mid-elevation plots (Figs. 3 and S6), although this may depend on LSF severity and time of occurrence. The POL-high plot (in southern Apennines) revealed the most resistant beech stand to LSFs without nPYs potentially associated to LSF impacts. In several cases, a defoliation-free portion of beech forest occurred above a defoliated one (e.g. at POL in 2016 or ACU and VOL in 2017). In these cases, the possibility of temperature inversions cannot be excluded, but the defoliation observed only at the intermediate zone of the slope suggested its relationship with the interannual thermal conditions and with the elevation dependent variations of bud burst timing.

At global scale, Zohner et al. (2020) found that the LSF risk for plants increases with elevation, due to higher intraday temperature variations, as it occurs in mountain areas. However, at our study sites with constrained elevation ranges, beech does not seem to present this pattern. The Apennine beech forests show similar risk of LSF damage along the elevational gradients as described in Lenz et al. (2013). Although beech in the Apennines rarely grows above the studied elevation range, we cannot exclude the possibility that below 1000 m a.s.l the LSF frequency induced defoliation could be lower.

Using two climate indices, we detected warm springs followed by frost events in eleven years. However, plots' mean chronologies showed an abrupt growth decrease in only six of those years. Ten out of the twelve plots were exposed by at least two extreme events in the 1950–2019 period (Fig. 3), with an average return time of 39 years, irregularly ranging from 13 to 60 years. Consecutive frost events occurred at the same site but causing damages at different elevations (e.g., ACU and VOL sites in 2016 and 2017 LSFs). No plots featured negative pointer years related to frosts in

consecutive years; however, in the VOL-mid 67 % of the series showed a negative event year in 2016 and 75 % of series in 2017. The estimation of the return time is highly influenced by the thresholds used to define a pointer year in tree-ring chronologies. Sangüesa-Barreda et al. (2021) calculated a reduced return time from 33 to 14 years before and after 1990, respectively. We found that most LSFs also occurred after 1990 (in 1991, 2001, 2016 and 2017), excluding the 1957 event which affected all sites (Fig. 4) and the 1970 event detected only at POL-low. In our stands the most severe LSFs occurred in 1957, 2016 and 2017, causing a radial growth reduction ranging between 36 % and 84 %. Even if in VOL-mid several trees were affected by consecutive frost events, their resilience values remained high even after the 2017 event.

LSFs can also occur at the beginning of dry growing seasons, a particular combination that occurred at the ACU site in 2017, with defoliation being observed only at mid elevation. Trees at ACU-mid show low resistance and resilience under the 2017 stressful conditions, with averaged values of 0.16 and 0.56 respectively (Table S7). Very dry summer periods can also reduce beech radial growth in the following years (Decuyper et al., 2020; Hacket-Pain et al., 2016).

However, excluding this effect at ACU site, we did not find significant growth reductions in the years following the LSFs (Fig. 4), suggesting a good recovery of beech to this disturbance, in accordance with recent studies (D'Andrea et al., 2019; Rubio-Cuadrado et al., 2021a, 2021b).

Not only LSF and drought events can cause negative pointer years in beech trees, but also masting years and insect outbreaks (Hacket-Pain et al., 2015; Camarero et al., 2018; Nussbaumer et al., 2021). The 2013 negative pointer year could be related to a mast year recorded across beech forests in central Italy (Mancini et al., 2016); however, the general lack of long-term, detailed data on seed production cannot confirm this hypothesis. In the same year, southern Apennine beech forests featured a radial growth



reduction which was attributed to unusually cold summer conditions (Šimůnek et al., 2021).

GLMMs did not detect significant elevation-dependent differences in LSF frequency. However, results suggest that the frequency of LSF rings could be more related to elevation rather than to individual tree parameters. A greater number of study sites and LSF events detected (by extending the analysis time period) are required to answer this question. In this sense, large remote-sensing analyses applied to relatively long periods can compensate the spatio-temporal biases (Bascietto et al., 2019). In the southern Apennines beech forests located within the altitudinal range of 1250–1500 m was the most exposed to the 2016 LSF (Nolè et al., 2018). This range corresponds to our mid-elevation plots (1245–1590 m) suggesting a high LSF sensitivity of this altitudinal belt in Apennine beech forests.

Detection and assessment of the LSFs impact on forest canopy cover and greenness can be efficiently conducted with remote sensing data and related indices (Bascietto et al., 2018, 2019; Nolè et al., 2018; Rubio-Cuadrado et al., 2021a; Olano et al., 2021). We found EVI being a more sensitive index than NDVI to detect LSF effects on beech canopies (Figs. 5 and 6). In the affected beech stands of our study in 2016 the average NDVI and EVI were respectively 30 % and 48 % lower than in unaffected forests, whereas in 2017 32 % and 47 % lower. The forest canopy on average recovered after 75 days from the frost events. However, the estimated recovery period can be biased by the time resolution of the used satellite data, and on cloud cover levels, challenging a correct daily resolution at population scale. The 2016 frost at VOL site was confirmed by the remoted sensed data, local meteorological records, and abrupt growth reductions, but not by the E-OBS gridded climate data that appeared to overestimate the minimum temperatures over the late frost period. The availability of suitable long-term in situ meteorological data would have helped to deepen into these analyses. However, microclimatic conditions play an important role in regulating the budburst timing in spring while temperature of buds and leaves can be much lower than the temperature recorded by standard climate stations during clear nights due to radiative cooling (Vitasse et al., 2021).

Software applications based on artificial intelligence can estimate the biophysical components of vegetation such as LAI, but they could underestimate higher LAI values such as those observed over dense forests (Brown et al., 2021; Filipponi, 2021). In our beech forests, LAI<sub>eff</sub> values ranged between 2.8 and 5.0 m<sup>2</sup> m<sup>-2</sup> in relation to the stand structure. LSFs in ACU and VOL sites resulted in an estimated loss of LAI<sub>eff</sub> values of 2.4–3.0 m<sup>2</sup> m<sup>-2</sup> compared to undamaged neighbouring plots. In many cases, affected plots showed lower LAI<sub>eff</sub> values until mid-July, probably due to the presence of smaller leaves (Rubio-Cuadrado et al., 2021a, 2021b). These findings demonstrate an intra-annual legacy effect which could be further investigated in terms of productivity or reduction in carbon uptake of the most affected stands by performing quantitative wood anatomy studies. Interestingly, such intra-annual legacy effects of reduced LAI<sub>eff</sub> did not turn into inter-annual growth legacy effects. The use of both high-resolution satellite and aerial multispectral images and LiDAR based sensors could provide more information to study forest disturbances at finer spatial and temporal scales.

Our findings cannot confirm that LSF severity increased in the 1990s, given the widespread and great impact of the 1957 LSF across the Apennines. Nonetheless, we demonstrated the high resilience capacity of beech forests after LSFs. In addition, we cannot discard that an increasing frequency of LSFs could alter such resilience capacity, particularly in Mediterranean mountains prone to a forecasted warming but also to more variable thermal conditions which could increase the frequency of adverse climate extremes such as frost and drought events (Giorgi and Lionello, 2008).

## 5. Conclusions

European beech low growth rates caused by LSF-induced leaf shedding depend on site spring phenology and abrupt spring temperature drop. However, beech trees affected by spring frost appeared to be resilient and

rapidly recovering their growth rates, showing no year-to-year legacy or carryover effects. Nonetheless, late frosts remain a threat to Apennine beech forests, especially if combined with summer drought, another major climate induced stress for this species. These extreme climate events and their potential synergy within globally warmer and more variable climate scenarios should be certainly considered in the future forest management and planning of mountain beech forests. The combination of remote sensing at broad scale and the finer tree-ring analyses could be applied to improve the detection of late spring frosts and to assess the LSFs impact and recovery time. In the context of climate change, the multiscale approach could improve the forecasting capacity of growth and canopy cover simulations after disturbances and climatic stressors.

## CRedit authorship contribution statement

**Enrico Tonelli:** Writing – original draft, Investigation, Methodology. **Alessandro Vitali:** Conceptualization, Investigation, Methodology, Writing – review & editing. **Francesco Malandra:** Investigation, Methodology, Writing – review & editing. **J. Julio Camarero:** Conceptualization, Investigation, Resources, Funding acquisition, Writing – review & editing. **Michele Colangelo:** Investigation, Writing – review & editing. **Angelo Nolè:** Investigation, Writing – review & editing. **Francesco Ripullone:** Writing – review & editing, Resources, Funding acquisition. **Marco Carrer:** Methodology, Writing – review & editing. **Carlo Urbinati:** Conceptualization, Writing – review & editing, Resources, Supervision, Funding acquisition.

## Data availability

Data will be made available on request.

## Declaration of competing interest

The authors declare that they have no known competing financial interests or personal relationships that could have appeared to influence the work reported in this paper.

## Acknowledgements

We acknowledge the E-OBS dataset from the EU-FP6 project UERRA (<https://www.uerra.eu>) and the Copernicus Climate Change Service, and the data providers in the ECA&D project (<https://www.ecad.eu>). JJC acknowledges funding by project RTI2018-096884-B-C31 of the Spanish Ministry of Economy, Industry and Competitiveness.

## Appendix A. Supplementary data

Supplementary data to this article can be found online at <https://doi.org/10.1016/j.scitotenv.2022.159239>.

## References

- Allevato, E., Saulino, L., Cesarano, G., Chirico, G.B., D'Urso, G., Falanga Bolognesi, S., Rita, A., Rossi, S., Saracino, A., Bonanomi, G., 2019. Canopy damage by spring frost in European beech along the Apennines: effect of latitude, altitude and aspect. *Remote Sens. Environ.* 225, 431–440. <https://doi.org/10.1016/j.rse.2019.03.023>.
- Augsburger, C.K., 2009. Spring 2007 warmth and frost: phenology, damage and refoliation in a temperate deciduous forest. *Funct. Ecol.* 23, 1031–1039. <https://doi.org/10.1111/j.1365-2435.2009.01587.x>.
- Augsburger, C.K., 2013. Reconstructing patterns of temperature, phenology, and frost damage over 124 years: spring damage risk is increasing. *Ecology* 94, 41–50. <https://doi.org/10.1890/12-0200.1>.
- Bascietto, M., Bajocco, S., Ferrara, C., Alivernini, A., Santangelo, E., 2019. Estimating late spring frost-induced growth anomalies in European beech forests in Italy. *Int. J. Biometeorol.* 63, 1039–1049. <https://doi.org/10.1007/s00484-019-01718-w>.
- Bascietto, M., Bajocco, S., Mazzenga, F., Matteucci, G., 2018. Assessing spring frost effects on beech forests in Central Apennines from remotely-sensed data. *Agric. For. Meteorol.* 248, 240–250. <https://doi.org/10.1016/j.agrformet.2017.10.007>.

- Bates, D., Mächler, M., Bolker, B.M., Walker, S.C., 2015. Fitting linear mixed-effects models using lme4. *J. Stat. Softw.* 67. <https://doi.org/10.18637/jss.v067.i01>.
- Bigler, C., Bugmann, H., 2018. Climate-induced shifts in leaf unfolding and frost risk of European trees and shrubs. *Sci. Rep.* 8. <https://doi.org/10.1038/s41598-018-27893-1>.
- Biondi, F., Qeadan, F., 2008. Inequality in paleorecords. *Ecology* 89, 1056–1067. <https://doi.org/10.1890/07-0783.1>.
- Bolte, A., Czajkowski, T., Kompa, T., 2007. The north-eastern distribution range of European beech - a review. *Forestry* <https://doi.org/10.1093/forestry/cpm028>.
- Briffa, K.R., Jones, D., 1990. *Basic chronology statistics and assessment*. Pages in E., editors *Methods of Dendrochronology*, pp. 137–153.
- Brown, L.A., Fernandes, R., Djamaï, N., Meier, C., Gobron, N., Morris, H., Canisius, F., Bai, G., Lerebourg, C., Lanconelli, C., Clerici, M., Dash, J., 2021. Validation of baseline and modified Sentinel-2 level 2 prototype processor leaf area index retrievals over the United States. *ISPRS J. Photogramm. Remote Sens.* 175, 71–87. <https://doi.org/10.1016/j.isprsjprs.2021.02.020>.
- Bunn, A.G., 2008. TECHNICAL NOTE a dendrochronology program library in R (dplR). *Dendrochronologia* 26, 115–124. <https://doi.org/10.1016/j.dendro.2008.01.002>.
- Camarero, J.J., Gazol, A., Sangüesa-Barreda, G., Cantero, A., Sánchez-Salguero, R., Sánchez-Miranda, A., Granda, E., Serra-Maluquer, X., Ibáñez, R., 2018. Forest growth responses to drought at short- and long-term scales in Spain: squeezing the stress memory from tree rings. *Front. Ecol. Evol.* 6. <https://doi.org/10.3389/fevo.2018.00009>.
- Camarero, J.J., Gazol, A., Sangüesa-Barreda, G., Vergarechea, M., Alfaro-Sánchez, R., Cattaneo, N., Vicente-Serrano, S.M., 2021. Tree growth is more limited by drought in rear-edge forests most of the times. *For. Ecosyst.* 8. <https://doi.org/10.1186/s40663-021-00303-1>.
- Caudullo, G., Welk, E., San-Miguel-Ayanz, J., 2017. Chorological maps for the main European woody species. *Data Brief* 12, 662–666. <https://doi.org/10.1016/j.dib.2017.05.007>.
- Chamberlain, C.J., Cook, B.I., Morales-Castilla, I., Wolkovich, E.M., 2021. Climate change reshapes the drivers of false spring risk across European trees. *New Phytol.* 229 (1), 323–334. <https://doi.org/10.1111/nph.16851>.
- Cook, E., Kairiukstis, L.A., 1990. *Tree-Ring Standardization and Growth-Trend Estimation, Methods of Dendrochronology*.
- Cornes, R.C., van der Schrier, G., van den Besselaar, E.J.M., Jones, P.D., 2018. An ensemble version of the E-OBS temperature and precipitation data sets. *J. Geophys. Res. Atmos.* 123, 9391–9409. <https://doi.org/10.1029/2017JD028200>.
- Cropper, J.P., 1979. Tree-ring skeleton plotting by computer. *Tree Ring Bull.* 39, 47–59.
- Čufar, K., Prislán, P., De Luis, M., Gričar, J., 2008. Tree-ring variation, wood formation and phenology of beech (*Fagus sylvatica*) from a representative site in Slovenia, SE Central Europe. *Trees Struct. Funct.* 22, 749–758. <https://doi.org/10.1007/s00468-008-0235-6>.
- D'Andrea, E., Rezaie, N., Battistelli, A., Gavrichkova, O., Kuhlmann, I., Matteucci, G., Moscatello, S., Proietti, S., Scartazza, A., Trumbore, S., Muhr, J., 2019. Winter's bite: beech trees survive complete defoliation due to spring late-frost damage by mobilizing old C reserves. *New Phytol.* 224, 625–631. <https://doi.org/10.1111/nph.16047>.
- D'Andrea, E., Rezaie, N., Prislán, P., Gričar, J., Collalti, A., Muhr, J., Matteucci, G., 2020. Frost and drought: effects of extreme weather events on stem carbon dynamics in a Mediterranean beech forest. *Plant Cell Environ.* 43. <https://doi.org/10.1111/pce.13858>.
- Dantec, C.F., Vitasse, Y., Bonhomme, M., Louvet, J.M., Kremer, A., Delzon, S., 2014. Chilling and heat requirements for leaf unfolding in European beech and sessile oak populations at the southern limit of their distribution range. *Int. J. Biometeorol.* 58. <https://doi.org/10.1007/s00484-014-0787-7>.
- Decuyper, M., Chávez, R.O., Čufar, K., Estay, S.A., Clevers, J.G.P.W., Prislán, P., Gričar, J., Črepinšek, Z., Merela, M., de Luis, M., Notivolj, R.S., del Castillo, E.M., Rozendaal, D.M.A., Bongers, F., Herold, M., Sass-Klaassen, U., 2020. Spatio-temporal assessment of beech growth in relation to climate extremes in Slovenia – an integrated approach using remote sensing and tree-ring data. *Agric. For. Meteorol.* 287. <https://doi.org/10.1016/j.agrformet.2020.107925>.
- Dittmar, C., Fricke, W., Elling, W., 2006. Impact of late frost events on radial growth of common beech (*Fagus sylvatica* L.) in Southern Germany. *Eur. J. For. Res.* 125, 249–259. <https://doi.org/10.1007/s10342-005-0098-y>.
- Dittmar, C., Zech, W., Elling, W., 2003. Growth variations of common beech (*Fagus sylvatica* L.) under different climatic and environmental conditions in Europe - a dendroecological study. *For. Ecol. Manag.* 173, 63–78. [https://doi.org/10.1016/S0378-1127\(01\)00816-7](https://doi.org/10.1016/S0378-1127(01)00816-7).
- Drusch, M., Del Bello, U., Carlier, S., Colin, O., Fernandez, V., Gascon, F., Hoersch, B., Isola, C., Laberinti, P., Martimort, P., Meygret, A., Spoto, F., Sy, O., Marchese, F., Bargellini, P., 2012. Sentinel-2: ESA's optical high-resolution mission for GMES operational services. *Remote Sens. Environ.* 120. <https://doi.org/10.1016/j.rse.2011.11.026>.
- Dukat, P., Bednorz, E., Ziemlińska, K., Urbaniak, M., 2022. Trends in drought occurrence and severity at mid-latitude European stations (1951–2015) estimated using standardized precipitation (SPI) and precipitation and evapotranspiration (SPEI) indices. *Meteorol. Atmos. Phys.* 134 (1), 1–21. <https://doi.org/10.1007/s00703-022-00858-w>.
- Filipponi, F., 2021. Comparison LAI estimates from high resolution satellite observations using different biophysical processors. Proceedings of the 1st International Electronic Conference on Agronomy, 3–17 May 2021. MDPI, Basel, Switzerland.
- Fritts, H.C., 1976. *Tree Rings and Climate*. Academic Press, London.
- Gazol, A., Camarero, J.J., 2022. Compound climate events increase tree drought mortality across European forests. *Sci. Total Environ.* 816. <https://doi.org/10.1016/j.scitotenv.2021.151604>.
- Gazol, A., Camarero, J.J., Colangelo, M., de Luis, M., Martínez del Castillo, E., Serra-Maluquer, X., 2019. Summer drought and spring frost, but not their interaction, constrain European beech and Silver fir growth in their southern distribution limits. *Agric. For. Meteorol.* 278. <https://doi.org/10.1016/j.agrformet.2019.107695>.
- Gefšler, A., Keitel, C., Kreuzwieser, J., Matyssek, R., Seiler, W., Rennenberg, H., 2007. Potential risks for European beech (*Fagus sylvatica* L.) in a changing climate. *Trees Struct. Funct.* 21, 1–11. <https://doi.org/10.1007/s00468-006-0107-x>.
- Giorgi, F., Lionello, P., 2008. Climate change projections for the Mediterranean region. *Glob. Planet. Chang.* 63, 90–104. <https://doi.org/10.1016/j.gloplacha.2007.09.005>.
- Hackett-Pain, A.J., Cavin, L., Friend, A.D., Jump, A.S., 2016. Consistent limitation of growth by high temperature and low precipitation from range core to southern edge of European beech indicates widespread vulnerability to changing climate. *Eur. J. For. Res.* 135, 897–909. <https://doi.org/10.1007/s10342-016-0982-7>.
- Hackett-Pain, A.J., Friend, A.D., Lagueard, J.G.A., Thomas, P.A., 2015. The influence of masting phenomenon on growth-climate relationships in trees: explaining the influence of previous summers' climate on ring width. *Tree Physiol.* 35, 319–330. <https://doi.org/10.1093/treephys/tpv007>.
- Heide, O.M., 1993. Dormancy release in beech buds (*Fagus sylvatica*) requires both chilling and long days. *Physiol. Plant.* 89, 187–191. <https://doi.org/10.1111/j.1399-3054.1993.tb01804.x>.
- Henrich, V., Jung, A., Götz, C., Sandow, C., Thürkow, D., Gläßer, C., 2009. Development of an online indices database: motivation, concept and implementation. 6th EARSeL Imaging Spectroscopy SIG Workshop Innovative Tool for Scientific and Commercial Environment Applications, pp. 16–18.
- Holmes, R., 1983. Computer-assisted quality control in tree-ring dating and measurement. *Tree-Ring Bull.* 43, 79–88.
- Huete, A., Didan, K., Miura, T., Rodriguez, E.P., Gao, X., Ferreira, L.G., 2002. Overview of the radiometric and biophysical performance of the MODIS vegetation indices. *Remote Sens. Environ.* 83, 195–213. [https://doi.org/10.1016/S0034-4257\(02\)00096-2](https://doi.org/10.1016/S0034-4257(02)00096-2).
- Jump, A.S., Hunt, J.M., Peñuelas, J., 2006. Rapid climate change-related growth decline at the southern range edge of *Fagus sylvatica*. *Glob. Chang. Biol.* 12, 2163–2174. <https://doi.org/10.1111/j.1365-2486.2006.01250.x>.
- Lamichhane, J.R., 2021. Rising risks of late-spring frosts in a changing climate. *Nat. Clim. Chang.* <https://doi.org/10.1038/s41558-021-01090-x>.
- Lenz, A., Hoch, G., Vitasse, Y., Körner, C., 2013. European deciduous trees exhibit similar safety margins against damage by spring freeze events along elevational gradients. *New Phytol.* 200, 1166–1175. <https://doi.org/10.1111/nph.12452>.
- Liu, H.Q., Huete, A., 1995. A feedback based modification of the NDVI to minimize canopy background and atmospheric noise. *IEEE Trans. Geosci. Remote Sens.* 33, 457–465. <https://doi.org/10.1109/tgrs.1995.8746027>.
- Lloret, F., Keeling, E.G., Sala, A., 2011. Components of tree resilience: effects of successive low-growth episodes in old ponderosa pine forests. *Oikos* 120, 1909–1920. <https://doi.org/10.1111/j.1600-0706.2011.19372.x>.
- Lough, J.M., Fritts, H.C., 1987. An assessment of the possible effects of volcanic eruptions on North American climate using tree-ring data, 1602 to 1900 A.D. *Clim. Chang.* 10, 219–239. <https://doi.org/10.1007/BF00143903>.
- Malandra, F., Vitali, A., Urbinati, C., Weisberg, P.J., Barbarino, M., 2019. Patterns and drivers of forest landscape change in the Apennines range, Italy. *Reg. Environ. Chang.* 19, 1973–1985. <https://doi.org/10.1007/s10113-019-01531-6>.
- Mancini, N.M., Mancini, G.M., Travaglini, D., Nocentini, S., Giannini, R., 2016. First Results on the Structure and Seed Production of Beech Stands at the Timberline in the Monti della Laga (Gran Sasso and Monti della Laga National Park). *Italia For. e Mont.* pp. 31–47. <https://doi.org/10.4129/ifm.2016.1.02>.
- Menzel, A., Seifert, H., Estrella, N., 2011. Effects of recent warm and cold spells on European plant phenology. *Int. J. Biometeorol.* 55, 921–932. <https://doi.org/10.1007/s00484-011-0466-x>.
- Nolè, A., Rita, A., Ferrara, A.M.S., Borghetti, M., 2018. Effects of a large-scale late spring frost on a beech (*Fagus sylvatica* L.) dominated Mediterranean mountain forest derived from the spatio-temporal variations of NDVI. *Ann. For. Sci.* 75, 1–11. <https://doi.org/10.1007/s13595-018-0763-1>.
- Nussbaumer, A., Gessler, A., Benham, S., de Cinti, B., Etzold, S., Ingerslev, M., Jacob, F., Lebourgeois, F., Levanić, T., Marjanović, H., Nicolas, M., Ostrogović Sever, M.Z., Prizwitzer, T., Rautio, P., Roskams, P., Sanders, T.G.M., Schmitt, M., Šrámek, V., Thimonier, A., Ukonmaanaho, L., Verstraeten, A., Vesterdal, L., Wagner, M., Waldner, P., Rigling, A., 2021. Contrasting resource dynamics in many years for European beech and oak—a continental scale analysis. *Front. For. Glob. Chang.* 4. <https://doi.org/10.3389/ffgc.2021.689836>.
- Olano, J.M., García-Cervigón, A.I., Sangüesa-Barreda, G., Rozas, V., Muñoz-Garachana, D., García-Hidalgo, M., García-Pedrero, Á., 2021. Satellite data and machine learning reveal the incidence of late frost defoliations on Iberian beech forests. *Ecol. Appl.* 31. <https://doi.org/10.1002/eap.2288>.
- Piovesan, G., Biondi, F., Di Filippo, A., Alessandrini, A., Maugeri, M., 2008. Drought-driven growth reduction in old beech (*Fagus sylvatica* L.) forests of the central Apennines, Italy. *Glob. Chang. Biol.* 14, 1265–1281. <https://doi.org/10.1111/j.1365-2486.2008.01570.x>.
- Pott, R., 2000. Palaeoclimate and vegetation - long-term vegetation dynamics in central Europe with particular reference to beech. *Phytocoenologia* 30, 285–333. <https://doi.org/10.1127/phyto/30/2000/285>.
- Rita, A., Camarero, J.J., Nolè, A., Borghetti, M., Brunetti, M., Pergola, N., Serio, C., Vicente-Serrano, S.M., Tramutoli, V., Ripullone, F., 2020. The impact of drought spells on forests depends on site conditions: the case of 2017 summer heat wave in southern Europe. *Glob. Chang. Biol.* 26, 851–863. <https://doi.org/10.1111/gcb.14825>.
- Rouse, J.W., Haas, R.H., Schell, J.A., Deering, D., 1973. Monitoring vegetation systems in the Great Plains with ERTS (Earth Resources Technology Satellite). *Third Earth Resources Technology Satellite-1 Symposium*, pp. 309–317.
- Rubio-Cuadrado, Á., Camarero, J.J., Rodríguez-Calcerrada, J., Perea, R., Gómez, C., Montes, F., Gil, L., 2021a. Impact of successive spring frosts on leaf phenology and radial growth in three deciduous tree species with contrasting climate requirements in central Spain. *Tree Physiol.* <https://doi.org/10.1093/treephys/tpab076>.
- Rubio-Cuadrado, Á., Gómez, C., Rodríguez-Calcerrada, J., Perea, R., Gordaliza, G.G., Camarero, J.J., Montes, F., Gil, L., 2021b. Differential response of oak and beech to late frost damage: an integrated analysis from organ to forest. *Agric. For. Meteorol.* 297. <https://doi.org/10.1016/j.agrformet.2020.108243>.
- Sangüesa-Barreda, G., Di Filippo, A., Piovesan, G., Rozas, V., Di Fiore, L., García-Hidalgo, M., García-Cervigón, A.I., Muñoz-Garachana, D., Baliva, M., Olano, J.M., 2021. Warmer springs have increased the frequency and extension of late-frost defoliations in southern

- European beech forests. *Sci. Total Environ.* 775. <https://doi.org/10.1016/j.scitotenv.2021.145860>.
- Schweingruber, F.H., Eckstein, D., Serre-Bachet, F., 1990. Identification, presentation and interpretation of event years and pointer years in dendrochronology. *Dendrochronologia* 8, 9–38.
- Serra-Maluquer, X., Gazol, A., Sangüesa-Barreda, G., Sánchez-Salguero, R., Rozas, V., Colangelo, M., Gutiérrez, E., Camarero, J.J., 2019. Geographically structured growth decline of rear-edge Iberian *Fagus sylvatica* forests after the 1980s shift toward a warmer climate. *Ecosystems* 22, 1325–1337. <https://doi.org/10.1007/s10021-019-00339-z>.
- Šimůnek, V., Vacek, Z., Vacek, S., Ripullone, F., Hájek, V., D'andrea, G., 2021. Tree rings of European beech (*Fagus sylvatica* L.) indicate the relationship with solar cycles during climate change in central and southern Europe. *Forests* 12. <https://doi.org/10.3390/f12030259>.
- Spinoni, J., Vogt, J.V., Naumann, G., Barbosa, P., Dosio, A., 2018. Will drought events become more frequent and severe in Europe? *Int. J. Climatol.* 38. <https://doi.org/10.1002/joc.5291>.
- Tognetti, R., Lasserre, B., Di Febbraro, M., Marchetti, M., 2019. Modeling regional drought-stress indices for beech forests in Mediterranean mountains based on tree-ring data. *Agric. For. Meteorol.* 265, 110–120. <https://doi.org/10.1016/j.agrformet.2018.11.015>.
- van der Maaten-Theunissen, M., van der Maaten, E., Bouriaud, O., 2015. PointRes: an R package to analyze pointer years and components of resilience. *Dendrochronologia* 35, 34–38. <https://doi.org/10.1016/j.dendro.2015.05.006>.
- Vitali, A., Urbinati, C., Weisberg, P.J., Urza, A.K., Garbarino, M., 2018. Effects of natural and anthropogenic drivers on land-cover change and treeline dynamics in the Apennines (Italy). *J. Veg. Sci.* 29, 189–199. <https://doi.org/10.1111/jvs.12598>.
- Vitasse, Y., Basler, D., 2013. What role for photoperiod in the bud burst phenology of European beech. *Eur. J. For. Res.* <https://doi.org/10.1007/s10342-012-0661-2>.
- Vitasse, Y., Baumgarten, F., Zohner, C.M., Kaewthongrach, R., Fu, Y.H., Walde, M.G., Moser, B., 2021. Impact of microclimatic conditions and resource availability on spring and autumn phenology of temperate tree seedlings. *New Phytol.* 232. <https://doi.org/10.1111/nph.17606>.
- Vitasse, Y., Bottero, A., Cailleret, M., Bigler, C., Fonti, P., Gessler, A., Lévesque, M., Rohner, B., Weber, P., Rigling, A., Wohlgemuth, T., 2019. Contrasting resistance and resilience to extreme drought and late spring frost in five major European tree species. *Glob. Chang. Biol.* 25. <https://doi.org/10.1111/gcb.14803>.
- Vitasse, Y., Delzon, S., Dufrêne, E., Pontaillet, J.Y., Louvet, J.M., Kremer, A., Michalet, R., 2009. Leaf phenology sensitivity to temperature in European trees: do within-species populations exhibit similar responses? *Agric. For. Meteorol.* 149. <https://doi.org/10.1016/j.agrformet.2008.10.019>.
- Vitasse, Y., Lenz, A., Körner, C., 2014. The interaction between freezing tolerance and phenology in temperate deciduous trees. *Front. Plant Sci.* 5. <https://doi.org/10.3389/fpls.2014.00541>.
- Weiss, M., Baret, F., 2016. S2ToolBox Level 2 products: LAI, FAPAR, FCOVER - Version 1.1. *Sentin. ToolBox Level2 Prod.* 53.
- Wigley, T.M.L., Briffa, K.R., Jones, P.D., 1984. On the average value of correlated time series with applications in dendroclimatology and hydrometeorology. *J. Clim. Appl. Meteorol.* 23, 201–213. [https://doi.org/10.1175/1520-0450\(1984\)023<0201:OTAVOC>2.0.CO;2](https://doi.org/10.1175/1520-0450(1984)023<0201:OTAVOC>2.0.CO;2).
- Xue, J., Su, B., 2017. Significant remote sensing vegetation indices: a review of developments and applications. *J. Sensors* <https://doi.org/10.1155/2017/1353691>.
- Zohner, C.M., Mo, L., Renner, S.S., Svenning, J.C., Vitasse, Y., Benito, B.M., Ordonez, A., Baumgarten, F., Bastin, J.F., Sebald, V., Reich, P.B., Liang, J., Nabuurs, G.J., De-Miguel, S., Alberti, G., Antón-Fernández, C., Balazy, R., Brändli, U.B., Chen, H.Y.H., Chisholm, C., Cienciala, E., Dayanandan, S., Fayle, T.M., Frizzera, L., Gianelle, D., Jagodzinski, A.M., Jaroszewicz, B., Jucker, T., Kepfer-Rojas, S., Khan, M.L., Kim, H.S., Korjus, H., Johannsen, V.K., Laarmann, D., Langn, M., Zawila-Niedzwiecki, T., Niklaus, P.A., Paquette, A., Pretzsch, H., Saikia, P., Schall, P., Seben, V., Svoboda, M., Tikhonova, E., Viana, H., Zhang, C., Zhao, X., Crowther, T.W., 2020. Late-spring frost risk between 1959 and 2017 decreased in North America but increased in Europe and Asia. *Proc. Natl. Acad. Sci. U. S. A.* 117. <https://doi.org/10.1073/pnas.1920816117>.
- Zohner, C.M., Rockinger, A., Renner, S.S., 2019. Increased autumn productivity permits temperate trees to compensate for spring frost damage. *New Phytol.* 221, 789–795. <https://doi.org/10.1111/nph.15445>.